Medium-Induced Gluon Radiation off Massive Quarks Fills the Dead Cone

Néstor Armesto, Carlos A. Salgado and Urs Achim Wiedemann

Theory Division, CERN, CH-1211 Geneva 23, Switzerland

February 7, 2008

We calculate the transverse momentum dependence of the medium-induced gluon energy distribution radiated off massive quarks in spatially extended QCD matter. In the absence of a medium, the distribution shows a characteristic mass-dependent depletion of the gluon radiation for angles $\theta < m/E$, the so-called dead cone effect. Medium-modifications of this spectrum are calculated as a function of quark mass m, initial quark energy E, in-medium pathlength and density. Generically, medium-induced gluon radiation is found to fill the dead cone, but it is reduced at large gluon energies compared to the radiation off light quarks. We quantify the resulting mass-dependence for momentum-averaged quantities (gluon energy distribution and average parton energy loss), compare it to simple approximation schemes and discuss its observable consequences for nucleus-nucleus collisions at RHIC and LHC. In particular, our analysis does not favor the complete disappearance of energy loss effects from leading open charm spectra at RHIC.

1. Introduction

Hadronic jets accompanying heavy quarks c, b differ from light quark and gluon initiated jets. These differences can be attributed to the suppression of gluon bremsstrahlung from massive charges at small angles $\theta < m/E$, the dead cone effect [1]. Observable consequences of this mass-dependence of the partonic fragmentation pattern include the softening of the light hadron spectra accompanying heavy quark jets [2], and the significant hardening of the leading charmed [3] or beauty [4] hadron. Mass-dependent dead cone conditions are implemented in the modified leading logarithmic approximation which accounts for jet multiplicity distributions [5]. They are also implemented in modern Monte Carlo simulations [6] which provide a probabilistic implementation of the perturbative part of the parton fragmentation process in the vacuum.

How is this parton fragmentation modified if the produced high-energy parent quark propagates through dense QCD matter, as is the case in ultrarelativistic nucleus-nucleus collisions at RHIC and at the LHC? As a first step towards

addressing this question [7], several groups [8–12] calculated to leading order in energy and for an arbitrary number of medium-induced momentum exchanges the modifications to the $q \to q\,g$ splitting process for energetic light quarks. These calculations indicate that medium effects can result in a significant additional energy degradation of the leading hadron which grows approximately linear with the density of the medium and approximately quadratic with the in-medium pathlength. Recent measurements [13–18] of high-$p_\perp$ hadroproduction and its centrality dependence in Au+Au collisions at $\sqrt{s_{\rm NN}} = 200$ GeV provide the first evidence [19] for this medium-induced parton energy loss. For light quarks and gluons, the formalism was also extended to the angular dependence of the medium-modified gluon radiation [20–23]. This allows to discuss medium modifications of jet shape and jet multiplicity observables [24].

For massive quarks, the formalism of medium-induced gluon radiation is not developed to the same extent. Dokshitzer and Kharzeev [25] suggested that the dead cone effect also reduces the medium-induced gluon radiation, thus resulting in a smaller suppression of leading charmed and beauty hadrons. They estimated this effect by multiplying the medium-induced gluon spectrum for massless quarks with a transverse momentum averaged suppression factor given in Eq. (4.16) below. However, the combination of vacuum-induced and medium-induced gluon energy distributions is known to differ significantly from a simple superposition [20] due to the non-trivial interplay of interference effects and elastic scattering. Hence, it is conceivable that the medium-induced part of the gluon radiation differs significantly from this averaged dead cone approximation. Going beyond this approximation may also be needed to distinguish mass-dependent final state effects from non-linear modifications of the initial gluon distribution for which open charm production may be a sensitive probe [26–29].

This motivates to parallel for the massive case the calculations of medium-induced gluon radiation which exist for the massless case. To this end, two groups [30–33] presented detailed calculations of parton energy loss for massive quarks. However, these calculations are limited to the average energy loss of massive quarks only. Here, we go beyond these studies i) by providing the first analysis of the double differential medium-induced gluon distribution as a function of transverse momentum and gluon energy and ii) by comparing this gluon distribution to the massless limit for a wide parameter range in quark mass, in-medium pathlength and medium density. In Section 2 we set up the path-integral formalism for parton energy loss. In Sections 3 and 4, we summarize the result of our numerical calculations and we provide simple analytical arguments for how the mass-dependence shows up in the medium-induced gluon radiation. The main results and their relevance for heavy quark production in nucleus-nucleus collisions at RHIC and LHC are discussed in the Conclusions.

2. Medium-induced Gluon Radiation off Massive Quarks: Formalism

The gluon distribution radiated from a massive quark traversing spatially extended QCD matter can be written as [10, 20]

$$\omega\frac{dI}{d\omega\, d\mathbf{k}_\perp} = \frac{\alpha_s\, C_F}{(2\pi)^2\,\omega^2}\, 2\mathrm{Re}\int_0^\infty dy_l \int_{y_l}^\infty d\bar{y}_l\, e^{i\bar{q}(y_l-\bar{y}_l)} \int d\mathbf{u}\, e^{-i\mathbf{k}_\perp\cdot\mathbf{u}}\, e^{-\frac{1}{2}\int_{\bar{y}_l}^\infty d\xi\, n(\xi)\,\sigma(\mathbf{u})} \times\frac{\partial}{\partial\mathbf{y}}\cdot\frac{\partial}{\partial\mathbf{u}}\int_{\mathbf{y}=0=\mathbf{r}(y_l)}^{\mathbf{u}=\mathbf{r}(\bar{y}_l)}\mathcal{D}\mathbf{r}\exp\left[i\int_{y_l}^{\bar{y}_l}d\xi\frac{\omega}{2}\left(\dot{\mathbf{r}}^2-\frac{n(\xi)\sigma\left(\mathbf{r}\right)}{i\,\omega}\right)\right]. \quad (2.1)$$

Here, ω and $\mathbf{k}_\perp$ denote the energy and transverse momentum of the emitted gluon, respectively. The Casimir factor $C_F = \frac{4}{3}$ determines the coupling strength of this gluon to the massive quark. For numerical results, we fix the coupling constant to $\alpha_s = 1/3$ unless stated otherwise. Eq. (2.1) resums the effects of arbitrary many medium-induced scatterings to leading order in $1/E$. Properties of the medium enter (2.1) via the product of the time-dependent density $n(\xi)$ of scattering centers times the strength of a single elastic scattering $\sigma(\mathbf{r})$. This dipole cross section $\sigma(\mathbf{r})$ is given in terms of the elastic high-energy cross section $|a(\mathbf{q})|^2$ of a single scatterer in the colour octet representation,

$$\sigma(\mathbf{r}) = 2\int\frac{d\mathbf{q}}{(2\pi)^2}\,|a(\mathbf{q})|^2\,\left(1-e^{-i\mathbf{q}\cdot\mathbf{r}}\right). \quad (2.2)$$

A detailed discussion of (2.1) including the physical interpretation of the *internal* integration variables (y_l, $\bar{y}_l$, $\mathbf{y}$, $\mathbf{u}$, ξ) can be found in Ref. [10].

The only mass-dependence of the gluon distribution (2.1) comes from the phase factor $\exp\left[i\bar{q}(y_l-\bar{y}_l)\right]$, where $\bar{q}$ is defined as the difference between the total three momentum of the initial quark (p_1), and the final quark (p_2) and gluon (k),

$$\bar{q} = p_1 - p_2 - k \simeq \frac{x^2\, m^2}{2\omega}, \qquad x = \frac{\omega}{E}. \quad (2.3)$$

For the abelian case, the same phase factor is known to give the mass-dependence of medium-induced photon radiation to leading order in $x \ll 1$, see Ref. [34, 35]. Paralleling the derivation of Ref. [10] for massive quarks, we have checked explicitly that this phase is the only mass dependence of the gluon distribution (2.1).

In the absence of medium effects, the gluon energy distribution (2.1) reduces to the unperturbed radiation I^{vac} associated to the production of a massive

quark in the vacuum. We write the full radiation spectrum as the sum of this vacuum component and its medium-modification $I^{\rm med}$,

$$\omega\frac{dI}{d\omega\, d\mathbf{k}_\perp} = \omega\frac{dI^{\rm vac}}{d\omega\, d\mathbf{k}_\perp} + \omega\frac{dI^{\rm med}}{d\omega\, d\mathbf{k}_\perp}\,. \tag{2.4}$$

By construction, both the full gluon distribution $\omega\frac{dI}{d\omega\, d\mathbf{k}_\perp}$, as well as the vacuum component $\omega\frac{dI^{\rm vac}}{d\omega\, d\mathbf{k}_\perp}$ have to be positive for all values of $k_\perp$ and ω. In contrast, the medium-induced modification $\omega\frac{dI^{\rm med}}{d\omega\, d\mathbf{k}_\perp}$ can be negative in some part of phase space: negative values correspond to a medium-induced depletion of the vacuum component.

In what follows, we calculate the medium-induced gluon distribution (2.1) in two different approximations. We limit the discussion to the case of a static medium with in-medium pathlength L for which

$$n(\xi) = n_0\,\Theta(L-\xi)\,. \tag{2.5}$$

From the analysis of Ref. [36], we expect that the case of an expanding medium can be reformulated in terms of a static medium (2.5) with suitably adjusted density n_0.

3. Opacity expansion

The opacity expansion of the gluon distribution (2.1) amounts to an expansion of the integrand of (2.1) in powers of $[n(\xi)\,\sigma(\mathbf{r})]^N$. Technical details of this expansion can be found in Appendix A and in Refs. [10, 11].

A. $N = 0$ vacuum term: the dead cone effect

In the absence of medium effects, $n(\xi) = 0$, the gluon distribution (2.1) reduces to the zeroth order in opacity,

$$\omega\frac{dI^{\rm vac}}{d\omega\, d\mathbf{k}_\perp} \equiv \omega\frac{dI(N=0)}{d\omega\, d\mathbf{k}_\perp} = \frac{\alpha_s\, C_F}{\pi^2} H(\mathbf{k}_\perp)\,, \tag{3.1}$$

where $H(\mathbf{k}_\perp)$ denotes the radiation term associated to the *hard* parton production,

$$H(\mathbf{k}_\perp) = \frac{\mathbf{k}_\perp^2}{\left(\mathbf{k}_\perp^2 + x^2 m^2\right)^2}\,. \tag{3.2}$$

By construction, this is the vacuum term in (2.4). It shows the dead cone effect: gluon radiation is suppressed for gluons which are emitted under small angles

$$\frac{\mathbf{k}_\perp^2}{\omega^2} < \frac{m^2}{E^2}\,. \tag{3.3}$$

The vacuum term (3.2) for the massive case vanishes for $k_\perp \to 0$, while the corresponding massless limit formally diverges like $\frac{1}{k_\perp^2}$.

B. $N = 1$ Opacity correction to the dead cone effect

We consider a medium of spatially extended QCD matter, modeled as a collection of colored Yukawa-type scattering centers (A.6) with Debye screening mass μ. To first order $N = 1$ in opacity, the average momentum transfer from the medium to the hard quark is μ.

Qualitative arguments: Consider a massless quark first. A gluon of energy ω decoheres from the wave function of this quark if its typical formation time $\bar{t}_{\rm coh} = \frac{2\omega}{\mu^2}$ is smaller than the typical distance L between the production point of the parton and the position of the scatterer. Hence, gluon radiation occurs if the phase

$$\bar{\gamma} = \frac{L}{\bar{t}_{\rm coh}} \equiv \frac{\bar{\omega}_c}{\omega}\,, \tag{3.4}$$

exceeds unity. Here, the characteristic gluon energy is

$$\bar{\omega}_c = \frac{1}{2}\mu^2\, L\,. \tag{3.5}$$

To discuss the transverse momentum dependence of gluon emission, we consider the corresponding $\mathbf{k}_\perp$-dependent phase accumulated due to scattering of the gluon,

$$\frac{\mathbf{k}_\perp^2}{2\omega} L = \frac{\bar{\kappa}^2}{\omega/\bar{\omega}_c} > 1\,, \tag{3.6}$$

where we use the rescaled transverse momentum

$$\bar{\kappa}^2 = \frac{\mathbf{k}_\perp^2}{\mu^2}\,. \tag{3.7}$$

For sufficiently large transverse momentum, the medium-induced gluon distribution will show the characteristic perturbative powerlaw for gluon production in a hard process,

$$\omega \frac{dI^{\rm med}_{m=0}}{d\omega\, d\bar{\kappa}^2} \propto \frac{1}{\bar{\kappa}^4} \qquad \text{for} \qquad \bar{\kappa} > 1\,. \tag{3.8}$$

This behavior can be checked in the $N = 1$ opacity expansion by taking the large-$\bar{\kappa}$ limit of Eq. (3.14) below. For transverse momentum $\bar{\kappa} < 1$, the gluon distribution levels off to a constant [24] which depends on $\omega/\bar{\omega}_c$. According to the condition (3.6), gluons can be emitted only for $\bar{\kappa}^2 > \frac{\omega}{\bar{\omega}_c}$. This allows to estimate from (3.8) the transverse momentum integrated gluon distribution in the region $\omega > \bar{\omega}_c$ where only $\bar{\kappa} > 1$ is relevant,

$$\omega \frac{dI^{\rm med}_{m=0}}{d\omega} \propto \int_{\omega/\bar{\omega}_c}^{\infty} \frac{d\bar{\kappa}^2}{\bar{\kappa}^4} \propto \frac{\bar{\omega}_c}{\omega} \qquad \text{for} \qquad \omega > \bar{\omega}_c\,. \tag{3.9}$$

This large-ω behavior has been established for the $N = 1$ opacity approximation [23, 37].

To estimate the mass-dependence of the gluon distribution, we first introduce the dead cone factor

$$F(\bar{\kappa}, \bar{M}) = \left(\frac{\bar{\kappa}^2}{\bar{\kappa}^2 + \bar{M}^2}\right)^2 = \left(\frac{\mathbf{k}_\perp^2}{\mathbf{k}_\perp^2 + x^2 m^2}\right)^2\,, \tag{3.10}$$

where

$$\bar{M}^2 = \frac{x^2 m^2}{\mu^2} = \frac{1}{2}\left(\frac{m^2}{E^2}\right)\frac{\bar{R}}{\bar{\gamma}^2}\,, \qquad \bar{R} = \bar{\omega}_c\, L\,. \tag{3.11}$$

For the vacuum term (3.1), this factor has the property that

$$\omega \frac{dI^{\rm vac}_{m}}{d\omega\, d\bar{\kappa}^2} = F(\bar{\kappa}, \bar{M})\, \omega \frac{dI^{\rm vac}_{m=0}}{d\omega\, d\bar{\kappa}^2}\,. \tag{3.12}$$

If the same estimate holds for the medium-induced part of the gluon radiation, then the distribution (3.8) is depleted for $\bar{\kappa}^2 < \max\left[\bar{\gamma}, \bar{M}^2\right]$. For the large-$\omega$ region, where $\bar{M}^2 > \bar{\gamma}$, the transverse momentum integrated gluon distribution can thus be estimated from (3.8),

$$\omega\frac{dI_m^{\rm med}}{d\omega} \propto \int_{\bar{M}^2}^{\infty}\frac{d\bar{\kappa}^2}{\bar{\kappa}^4} \propto \left(\frac{m^2}{E^2}\right)\bar{R}\frac{\bar{\omega}_c^2}{\omega^2} \quad \text{for} \quad \omega > \bar{\omega}_c/\left(\frac{m^2}{E^2}\bar{R}\right)^{1/3}. \tag{3.13}$$

This distribution drops off faster ($\propto \frac{1}{\omega^2}$) than the corresponding massless term (3.9). We thus expect a mass-dependent depletion of the medium-induced gluon radiation at large gluon energy. We emphasize that the dead cone suppression is a sufficient but not a necessary condition for this large-ω behavior. What is needed is only that mass effects regulate the singularity $\frac{1}{\bar{\kappa}^4}$ on a scale $\bar{M}$. Since the phase space for $\bar{\kappa}^2 < \bar{M}^2$ is small, it is not essential whether this regulation occurs by complete extinction of the radiation e.g. via $F(\bar{\kappa}, \bar{M})$, or whether the dead cone is filled by a finite non-singular spectrum for $\bar{\kappa}^2 < \bar{M}^2$. We shall find that the latter case is realized.

Quantitative analysis: We have calculated the medium modification of the gluon energy distribution (2.4) to first order in opacity, see Appendix A. In the massless limit, our result reduces to the $N = 1$ opacity result given in Ref. [10]. For finite in-medium path-length L, it interpolates between the totally coherent and totally incoherent limiting cases of the gluon radiation spectrum. In particular, the incoherent limit is an independent superposition of three distinct radiation terms: the hard radiation term (3.2) shifted to $H(\mathbf{k}+\mathbf{q})$ due to elastic scattering, a Gunion-Bertsch radiation term associated to gluon production due to a single scattering center well separated from the quark production, and a probability conserving third term (see Appendix A). In terms of the dimensionless variables introduced above, the medium-modified gluon distribution to first order in opacity is

$$\begin{aligned}\omega\frac{dI(N=1)}{d\omega\, d\bar{\kappa}^2} = \frac{\alpha_s\, C_F}{\pi}(2\, n_0\, L)\int_0^{\infty} d\bar{q}^2 \frac{\left(\bar{q}^2+\bar{M}^2\right) - \frac{1}{\bar{\gamma}}\sin\left[\bar{\gamma}\left(\bar{q}^2+\bar{M}^2\right)\right]}{\left(\bar{q}^2+\bar{M}^2\right)^2} \\ \times\frac{\bar{q}^2}{\bar{q}^2+\bar{M}^2}\frac{\left(\bar{\kappa}^2+\bar{M}^2\right)+\left(\bar{\kappa}^2-\bar{M}^2\right)\left(\bar{\kappa}^2-\bar{q}^2\right)}{\left(\bar{\kappa}^2+\bar{M}^2\right)\left[\left(1+\bar{\kappa}^2+\bar{q}^2\right)^2-4\bar{\kappa}^2\bar{q}^2\right]^{3/2}}.\end{aligned} \tag{3.14}$$

The medium-induced gluon energy distribution is obtained by integrating (3.14) over transverse momentum up to the kinematic boundary $k = \omega$. In terms of the integration variable $\bar{\kappa}^2$, this corresponds to

$$\omega\frac{dI(N=1)}{d\omega} = \int_0^{\bar{R}/2\bar{\gamma}^2} d\bar{\kappa}^2\omega\frac{dI(N=1)}{d\omega\, d\bar{\kappa}^2}, \tag{3.15}$$

where the integration boundary is written in terms of $\bar{R} = \bar{\omega}_c\, L$. The integral of (3.15) over gluon energy defines the average medium-induced energy loss

$$\langle \Delta E_{\rm ind} \rangle = \int_0^E d\omega\, \omega \frac{dI(N=1)}{d\omega}\,. \tag{3.16}$$

In the $L \to \infty$ limit, equation (3.16) coincides with the expression given by Djordjevic and Gyulassy [32]. At finite in-medium pathlength L, the differences between (3.16) and Ref. [32] may be due to the use of a different density distribution $n(\xi)$ of scattering centers.

C. Numerical results

Explored parameter space: The double differential gluon distribution (3.14) for massless quarks depends on two parameters only, the characteristic gluon energy $\bar{\omega}_c$ and the typical transverse momentum (Debye screening mass) μ. Presenting our results in rescaled variables $\bar{\kappa}^2 = \mathbf{k}_\perp^2/\mu^2$ and $\bar{\gamma} = \bar{\omega}_c/\omega$, we explore the unrestricted parameter range for $\bar{\omega}_c$ and μ^2. For the transverse momentum integrated gluon distribution (3.15), the parameter $\bar{R} = \bar{\omega}_c\, L$ enters via the integration boundary. We motivate our choice of the value of $\bar{R}$ from a model analysis of high-$p_\perp$ suppressed hadroproduction in central Au-Au collisions at RHIC. The order of magnitude of the suppression is in qualitative agreement with the parameter choice $\bar{R} = 2000$, $\bar{\omega}_c = 67.5$ GeV, and $n_0\, L = 1$, see Ref. [23]. We thus choose $\bar{R} = 1000$ and a significantly larger value $\bar{R} = 40000$ for numerical calculations. The latter can be viewed as an upper estimate for LHC. If the quark mass is finite, the double differential gluon distribution also depends on the effective mass (3.11) which is a function of the ratio m/E and of $\bar{R}$. We prefer to present all results in terms of m/E and $\bar{R}$ although they appear in (3.14) only in one combination.

Results: We studied the differences between the medium-induced gluon distribution (3.14) radiated off massive quarks, and the corresponding double differential gluon distribution for massless quarks

$$\lim_{m\to 0} \omega \frac{dI(N=1)}{d\omega\, d\bar{\kappa}^2} = \frac{\alpha_s\, C_F}{\pi} (2\, n_0\, L) \int_0^\infty d\bar{q}^2 \frac{\bar{q}^2 - \frac{1}{\bar{\gamma}} \sin\left(\bar{\gamma}\bar{q}^2\right)}{\bar{q}^4} \times \frac{(1+\bar{\kappa}^2-\bar{q}^2)}{\left[(1+\bar{\kappa}^2+\bar{q}^2)^2 - 4\bar{\kappa}^2\bar{q}^2\right]^{3/2}}\,. \tag{3.17}$$

Also, we tested the conjecture that the medium-induced distribution can be obtained from the massless expression by multiplying with a dead cone factor (3.10),

$$\omega \frac{dI_{\rm dead}(N=1)}{d\omega\, d\bar{\kappa}^2} = F(\bar{\kappa}, \bar{M}) \lim_{m\to 0} \omega \frac{dI(N=1)}{d\omega\, d\bar{\kappa}^2}\,. \tag{3.18}$$

Fig. 1 shows that the transverse momentum dependence of the medium-induced gluon distribution deviates qualitatively from the dead cone approximation (3.18). At small transverse momentum, the medium-induced radiation does not vanish as for the dead cone approximation (3.18). In contrast, it is enhanced compared to the massless case.

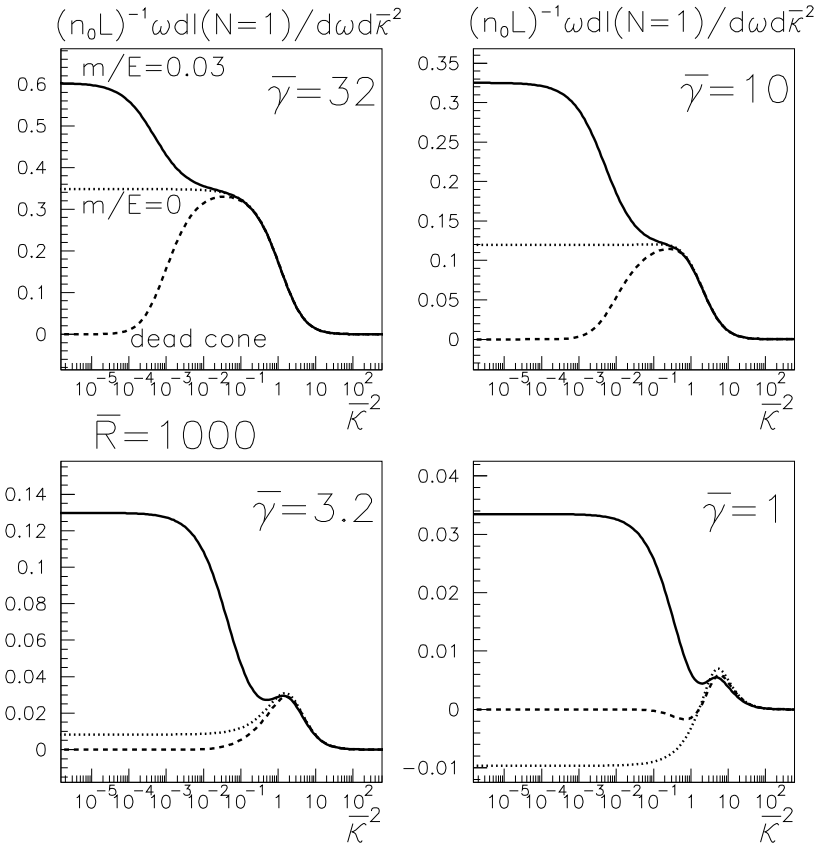

Fig. 1. The medium-induced gluon energy distribution as a function of the transverse momentum $\bar{\kappa}^2 = \mathbf{k}_\perp^2/\mu^2$ and for different values of $\bar{\gamma} = \bar{\omega}_c/\omega$. Different curves correspond to the full medium-induced gluon distribution (3.14) for a mass to energy ratio 0.03 of the heavy quark (solid line), the massless limit (3.17) of this spectrum (dotted line), and its dead cone approximation (3.18) (dashed line).

For a more detailed discussion of Fig. 1, we first note that the mass to energy ratio $\frac{m}{E}$ and the parameter $\bar{R}$ enter the double differential gluon distribution only via the effective mass parameter $\bar{M}^2 = \frac{1}{2}\frac{m^2}{E^2}\frac{\bar{R}}{\bar{\gamma}^2}$, see (3.11). For the numerical values in Fig. 1, we find $\bar{M}^2 = 0.45/\bar{\gamma}^2$. In accordance with the qualitative arguments given in Section 3 B, mass-dependent deviations are seen to become significant for transverse momentum $\bar{\kappa}^2 < \bar{M}^2$. In particular, for smaller gluon energies ω, i.e. for larger values of $\bar{\gamma} = \frac{\bar{\omega}_c}{\omega}$, the onset of mass-dependent deviations is at smaller values of $\bar{\kappa}^2$. On the other hand, for larger gluon energy (i.e. for small $\bar{\gamma}$), the transverse momentum distribution of the radiation

spectrum can exceed the Debye screening mass significantly. The condition $\bar{\kappa}^2 < 1$ provides only a rough estimate for the upper limit on medium-induced gluon radiation.

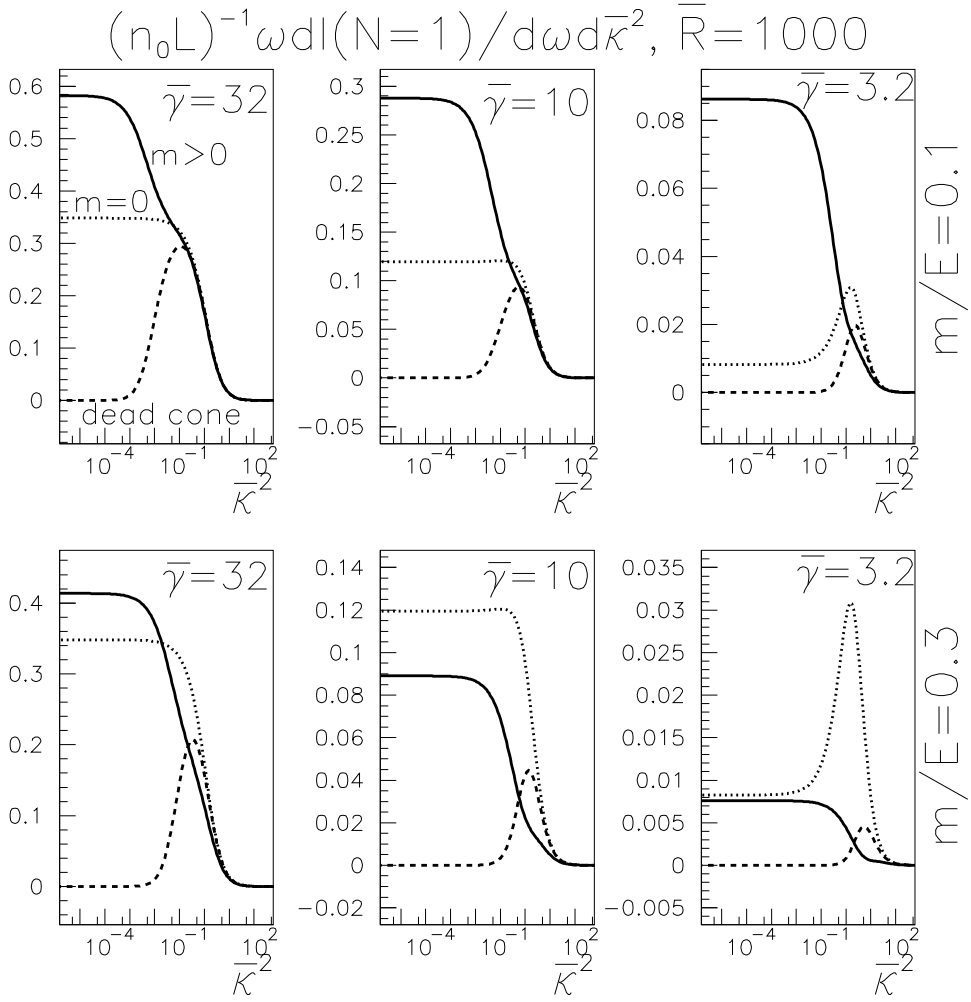

Fig. 2. Same as Fig. 1 but for the larger mass to energy ratios $\frac{m}{E} = 0.1$ and $\frac{m}{E} = 0.3$.

We next comment on the origin of the mass dependence in Fig. 1 which is in qualitative disagreement with the dead cone prescription (3.18). For massless quarks, medium modifications of the gluon radiation are known to be determined by two competing effects [20]: First, additional medium-induced gluon radiation increases the gluon distribution. Second, medium-induced elastic scattering shifts emitted gluons to larger transverse momentum and thus depletes the $\propto \frac{1}{k_\perp^2}$ vacuum distribution at small transverse momentum. [For very energetic gluons which are emitted predominantly at small angle, the second mechanism dominates and the medium-induced part of the gluon distribution is hence negative for small transverse momentum. This is seen in the plot for

$\bar{\gamma} = 1$ in Fig. 1.] For massive quarks, the dead cone effect implies that there is no vacuum distribution at small angle which can be depleted due to elastic scattering. As a consequence, for massive quarks the second mechanism does not apply at small $\bar{\kappa}$ and the gluon radiation is further enhanced.

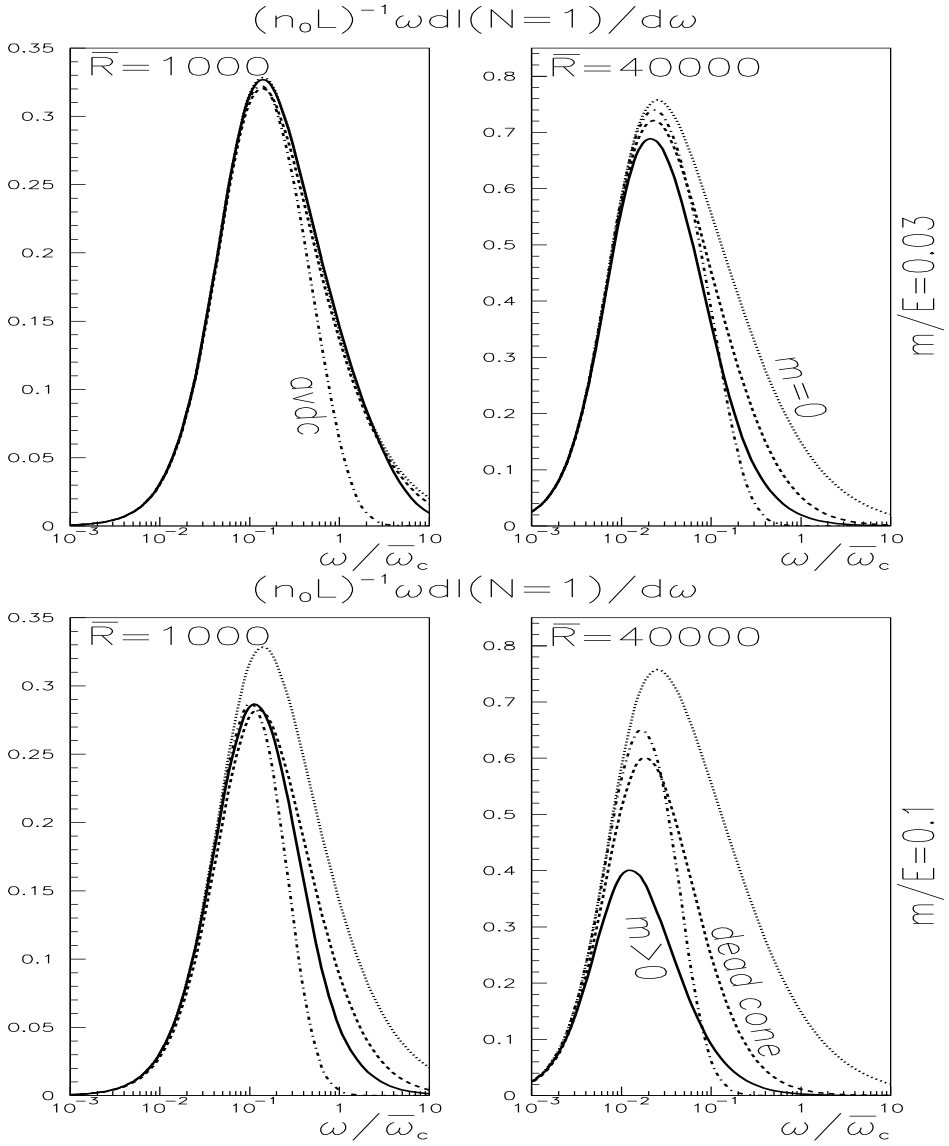

Fig. 3. The medium-induced gluon energy distribution (3.15) calculated from the full expression (3.14) for a massive quark (solid line), from the massless limit (3.17) (dotted line), from the dead-cone approximation (3.18) (dashed line) and from the average dead cone factor (3.19) multiplied by the massless spectrum (dash-dotted line).

We have varied the mass to energy ratio $\frac{m}{E}$ and the parameter $\bar{R}$ in our calculation over a wide parameter range ($0.001 < \frac{m}{E} < 0.3$ and $1000 < \bar{R} < 40000$). Quantitatively, the medium-induced radiation varies significantly with these

parameters (see the discussion below). Qualitatively, the effect discussed above is generic for the entire parameter space: For transverse momentum $\bar{\kappa} < \bar{M}$, medium-induced gluon radiation fills the dead cone. For a significant part of the parameter space, it is enhanced compared to the massless case, too. For very large mass to energy ratios, however, mass effects limit significantly the medium-induced gluon radiation and the radiation from massless quarks finally dominates for $\bar{\kappa} < \bar{M}$, see Fig. 2.

The phase space of the dead cone region $\bar{\kappa}^2 < \bar{M}^2$ is small. For massive quarks, neither the vacuum contribution nor the medium-induced contribution to (2.4) contain collinear singularities which could enhance the importance of this phase space region. As a consequence, parton energy loss off hard quarks will be dominated mainly by radiation in the region $\bar{\kappa}^2 > \bar{M}^2$. For large $\bar{\kappa}$, however, the medium-induced radiation off massive quarks (3.14) is suppressed compared to the massless limit if the $\frac{m}{E}$-ratio is sufficiently large, see Fig. 2. This feature dominates the transverse momentum integrated gluon energy distribution (3.15), see Fig. 3. In particular, the radiation is depleted for large gluon energy, since it increases with the effective mass parameter $\bar{M}^2 = \frac{1}{2}\frac{m^2}{E^2}\bar{R}\frac{\omega^2}{\bar{\omega}_c^2}$. Fig. 3 indicates that the mass-dependent suppression of (3.15) is even stronger than predicted by the dead cone approximation (3.18).

One may ask whether the correct amount of mass-dependent suppression can be estimated from a $\bar{\kappa}$-independent suppression factor $F_{\rm avdc}(\bar{M})$ multiplying the gluon energy distribution for massless quarks. [Here, the subscript "avdc" stands for "average dead cone".] Such a factor could be useful for simplified calculations in which $\mathbf{k}_\perp$-dependent information is not available. Paralleling an estimate given in Ref. [25] for the dipole approximation [see Eq. (4.16) below], we have estimated $F_{\rm avdc}(\bar{M})$ by evaluating the dead cone factor (3.7) for the characteristic angle under which medium-induced gluon radiation occurs, $\theta_c^2 = \frac{\mu^2}{\omega^2} = \left(\frac{\bar{\omega}_c}{\omega}\right)^2 \frac{1}{\bar{R}}$. We find

$$F_{\rm avdc}(\bar{M}) = \left(\frac{1}{1+\bar{M}^2}\right)^2 . \tag{3.19}$$

Substituting this average for the dead-cone factor in (3.18) and calculating the transverse momentum integrated spectrum, one tends to overestimate the mass-dependent reduction of the medium-induced radiation, see Fig. 3.

Fig. 4 shows the ratio of the medium-induced average parton energy loss (3.16) for massive quarks, normalized to the same quantity calculated for massless quarks. In general, a finite quark mass is found to reduce the parton energy loss and this reduction increases strongly with $\frac{m}{E}$.

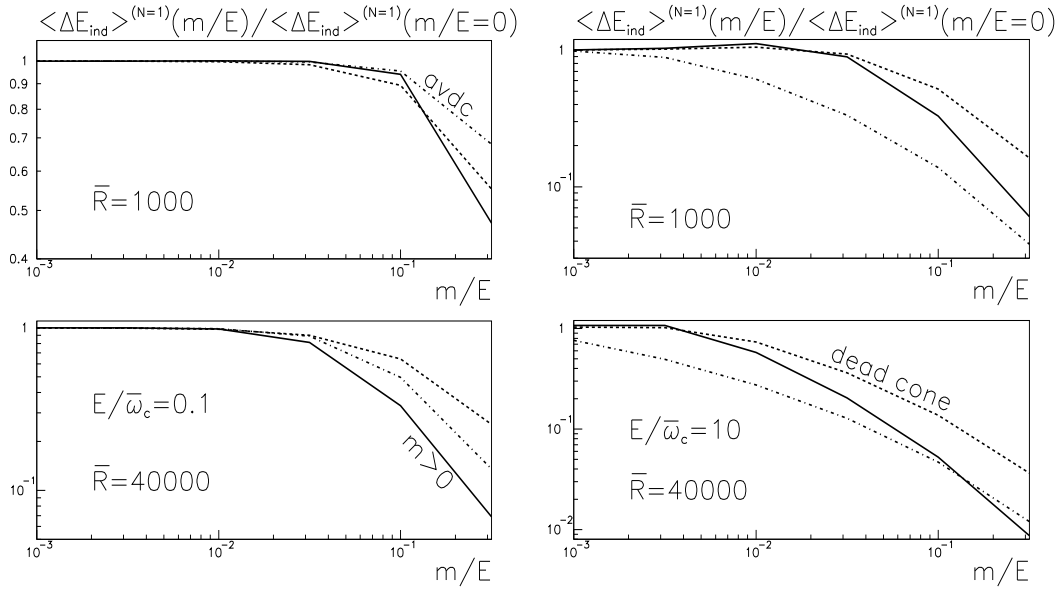

Fig. 4. The average medium-induced parton energy loss (3.16) for massive quarks, normalized to the massless limit, for different values of the density parameter $\bar{R} = \bar{\omega}_c L$. Curves are calculated for the full medium-induced radiation (3.14) off massive quarks (solid lines), the dead cone approximation (3.18) (dashed lines) and the corresponding expression with averaged dead cone (3.19) (dash-dotted lines).

We now discuss in more detail the main theoretical uncertainty entering (3.16) and Fig. 4. Since the double differential distribution (3.14) is calculated in the eikonal approximation, it can have support for gluon energies $\omega > E$. This just indicates the limited validity of the eikonal approximation for small energies E. This issue is critical for calculations of the average parton energy loss (3.16) which can depend strongly on the phase space limit $\frac{\omega}{\bar{\omega}_c} < \frac{E}{\bar{\omega}_c}$ imposed on the integral over the gluon energy distribution. In Fig. 5, we illustrate this point by showing the gluon energy distribution and the average energy loss (3.16) for the parameter set $n_0 L = 4$, $\mu = 500$ MeV, $L = 4$ fm and $\alpha_s = 0.3$. This parameter set was used to reproduce the suppression of high-$p_\perp$ hadroproduction observed in Au+Au collisions at RHIC [38], and it is used in the numerical calculation of Ref. [32] together with a charm quark mass of $m = 1.5$ GeV. For the standard upper integration bound $\omega < E$, the massive case agrees qualitatively in magnitude and energy dependence with the calculation shown in Fig. 1 of Ref. [32]. Small quantitative differences are due to the different finite L dependence of the density distributions, as argued following Eq. (3.16). However, as seen in Fig. 5, the average energy loss (3.16) off massless quarks turns out to be smaller since a larger part of the gluon energy distribution lies above the kinematic cut. We have made no attempt to remedy this possibly unphysical behavior. We simply emphasize that any *a posteriori* modification of the large-ω tail of $\omega \frac{dI}{d\omega}$ entails significant theoretical

uncertainties. It is an open problem of obvious importance to include finite energy constraints on the level of the radiation spectrum (i.e. on the level of multiple scattering Feynman diagrams) rather than on the level of the integrated parton energy loss.

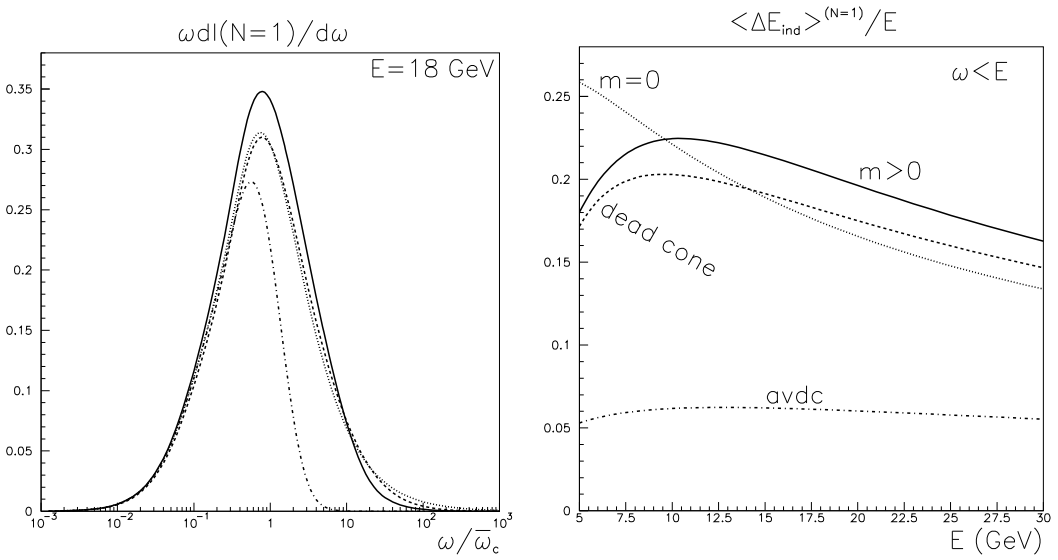

Fig. 5. For finite quark energy E, the normalized average energy loss (rhs) depends significantly on the kinematic boundary up to which the gluon energy distribution (lhs) is integrated. This entails significant uncertainties, which are discussed in the text. Parameter values are taken from Ref. [32].

4. Dipole approximation (multiple soft scattering)

If the medium provides a large number of soft momentum transfers, rather than a few harder ones, then the projectile performs a Brownian motion in transverse momentum. This case can be studied in the saddle point approximation of the path-integral (2.1), using [34, 39]

$$n(\xi)\,\sigma(\mathbf{r}) \simeq \frac{1}{2}\,\hat{q}(\xi)\,\mathbf{r}^2\,. \tag{4.1}$$

Here, $\hat{q}(\xi)$ is the transport coefficient [8] which characterizes the medium-induced transverse momentum squared $\langle q_\perp^2 \rangle$ transferred to the projectile per unit path length λ. In the approximation (4.1), the path integral in (2.1) is equivalent to that of a harmonic oscillator which allows for an explicit calculation.

A. The Vacuum Term shows the Dead Cone Effect

For the transport coefficient $\hat{q}(\xi) = \hat{q}\Theta(L-\xi)$ of a static medium of length L, we evaluate the gluon distribution (2.1) by splitting the longitudinal integrals into three parts [35],

$$\begin{aligned}\omega\frac{dI}{d\omega\, d\kappa^2} &= \omega\frac{dI_4}{d\omega\, d\kappa^2} + \omega\frac{dI_5}{d\omega\, d\kappa^2} + \omega\frac{dI_6}{d\omega\, d\kappa^2} \\ &= \int_0^L dy_l \int_{y_l}^L d\bar{y}_l \ldots + \int_0^L dy_l \int_L^\infty d\bar{y}_l \ldots + \int_L^\infty dy_l \int_{y_l}^\infty d\bar{y}_l \ldots \end{aligned} \tag{4.2}$$

In complete analogy to the calculation for the massless case [20], one can shown that the term I_6 does not depend on the medium and takes the form

$$\omega\frac{dI_6}{d\omega\, d\mathbf{k}_\perp} = \frac{\alpha_s\, C_F}{\pi^2}\frac{\mathbf{k}_\perp^2}{\left(\mathbf{k}_\perp^2 + x^2 m^2\right)^2}\,. \tag{4.3}$$

This expression coincides with the vacuum term (3.1). In the multiple soft scattering separation, there is hence a simple separation of the gluon distribution (2.4) into the vacuum term (4.3) and the medium-induced contribution $I_4 + I_5$. The latter vanish in the absence of a medium, $\hat{q} = 0$.

B. Medium-induced gluon radiation

We now discuss the medium-induced part of the gluon distribution (2.4) which in the multiple soft scattering (mss) approximation takes the form

$$\omega\frac{dI^{\rm mss}}{d\omega\, d\kappa^2} = \omega\frac{dI_4}{d\omega\, d\kappa^2} + \omega\frac{dI_5}{d\omega\, d\kappa^2}\,. \tag{4.4}$$

The terms I_4 and I_5 are defined in (4.2) and are given explicitly in Appendix B.

Qualitative arguments: Consider first the qualitative behavior of (4.4) for the case of a massless quark. The energy and transverse momentum scales which determine medium-induced gluon radiation can be estimated in analogy to the discussion given for the $N = 1$ opacity case. The phase accumulated by the gluon due to multiple scattering is given in terms of the characteristic gluon energy ω_c [40],

$$\gamma = \left\langle \frac{k_\perp^2}{2\omega}\,\Delta z \right\rangle \sim \frac{\hat{q}\, L}{2\omega} L = \frac{\omega_c}{\omega}\,, \qquad \omega_c = \frac{1}{2}\,\hat{q}\, L^2\,. \tag{4.5}$$

This phase should be larger than $\gamma \sim O(1)$ for the gluon to decohere from the massless quark. Here, we have used that the gluon carries a typical transverse momentum squared of order $\langle \mathbf{k}_\perp^2 \rangle \sim \hat{q}\, L$. We express the transverse momentum $\mathbf{k}_\perp$ in units of this characteristic scale,

$$\kappa^2 = \frac{\mathbf{k}_\perp^2}{\hat{q}\, L}\,. \tag{4.6}$$

For the case of many soft scattering centers, several centers act coherently if the formation time of the gluon exceeds its mean free path. The typical transverse momentum accumulated by the gluon is then $\mathbf{k}_\perp^2 \simeq \langle q_\perp^2 \rangle \, \frac{t_{\rm form}}{\lambda} = \hat{q}\, t_{\rm form}$ while its formation time is $t_{\rm form} \simeq \frac{\omega}{\mathbf{k}_\perp^2}$. Medium-induced radiation thus relates transverse momentum and gluon energy,

$$\mathbf{k}_\perp^2 \simeq \sqrt{\hat{q}\,\omega} \qquad \text{or in dimensionless units:} \qquad \kappa^2 \simeq \sqrt{\frac{1}{2\,\gamma}}\,. \tag{4.7}$$

On the other hand, the number of scattering centers which act coherently is $N_{\rm coh} = \frac{t_{\rm form}}{\lambda}$. For $N_{\rm coh} > 1$, the medium-induced gluon radiation in the multiple soft scattering limit reads

$$\omega \frac{dI^{\rm mss}_{m=0}}{d\omega\, d\kappa^2} \simeq \frac{L}{\lambda\, N_{\rm coh}}\, \omega \frac{dI^{\rm 1scatt}_{m=0}}{d\omega\, d\kappa^2}\,, \tag{4.8}$$

where $I^{\rm 1scatt}_{m=0}$ is the radiation off a single scattering center and the total number L/λ of scattering centers along the path of extension L is reduced by coherence effects to the effective number

$$\frac{L}{\lambda\, N_{\rm coh}} \sim \sqrt{\frac{\omega_c}{\omega}} \sim \frac{1}{\kappa^2}\,. \tag{4.9}$$

If the gluon energy is small, $\omega < \omega_c$, then it follows from (4.7) that $\kappa^2 < 1$. The transverse momentum integral over $\omega \frac{dI^{\rm 1scatt}_{m=0}}{d\omega\, d\kappa^2}$ gives an energy-independent function and we find from (4.8) and (4.9) that

$$\omega \frac{dI^{\rm mss}_{m=0}}{d\omega} \propto \frac{L}{\lambda\, N_{\rm coh}} \sim \sqrt{\frac{\omega_c}{\omega}} \qquad \text{for} \qquad \omega < \omega_c\,. \tag{4.10}$$

For $\kappa^2 > 1$, on the other hand, the spectrum $\omega \frac{dI^{\rm 1scatt}_{m=0}}{d\omega\, d\kappa^2}$ is characterized again by the perturbative tail (3.8). Combining this information with Eqs. (4.8) and (4.9), one obtains

$$\omega \frac{dI^{\rm mss}_{m=0}}{d\omega} \sim \int_{\omega/\omega_c}^{\infty} \frac{d\kappa^2}{\kappa^6} \sim \left(\frac{\omega_c}{\omega}\right)^2 \qquad \text{for} \qquad \omega > \omega_c\,. \tag{4.11}$$

Both limiting cases, (4.10) and (4.11) agree with the results of the full calculation [23] in the multiple soft scattering limit for massless quarks.

To estimate the mass-dependence of the gluon distribution, we parallel the discussion of Section 3 B. We introduce the dead cone factor

$$F(\kappa, M) = \left(\frac{\kappa^2}{\kappa^2 + M^2}\right)^2 = \left(\frac{\mathbf{k}_\perp^2}{\mathbf{k}_\perp^2 + x^2 m^2}\right)^2 , \tag{4.12}$$

where

$$M^2 = \frac{x^2 m^2}{\hat{q} L} = \frac{1}{2}\left(\frac{m^2}{E^2}\right) R \frac{\omega^2}{\omega_c^2} , \qquad R = \omega_c \, L . \tag{4.13}$$

Restricting the κ^2-integration of the perturbative tail by this mass term, we find

$$\omega \frac{dI_m^{\rm mss}}{d\omega} \sim \int_{M^2}^{\infty} \frac{d\kappa^2}{\kappa^6} \sim \frac{1}{M^4} , \qquad \text{for} \qquad \omega > \omega_c . \tag{4.14}$$

In close analogy to the estimate for single hard scattering in Section 3, the large-ω region drops off significantly faster than for the massless case (4.11). We thus expect a mass-dependent depletion for large ω.

C. Numerical results

Explored parameter space: In analogy to the study in Section 3 C, we present all results in rescaled variables κ^2 and γ. The parameter $R = \omega_c \, L$ is explored for the values 1000 and 40000. See Section 3 C for further details.

Results: We have calculated the transverse momentum dependence of the medium-induced gluon distribution (4.4) in the multiple soft scattering approximation. We have compared this distribution to the massless limit and to the dead cone approximation

$$\omega \frac{dI_{\rm dead}^{\rm mss}}{d\omega \, d\kappa^2} = F(\kappa, M) \, \omega \frac{dI_{m=0}^{\rm mss}}{d\omega \, d\kappa^2} . \tag{4.15}$$

As seen in Fig. 6, the results are in qualitative agreement with those obtained in the opacity expansion (see Fig. 3 and Section 3 C for discussion). In particular, we find that the dead cone is filled by medium-induced gluon radiation. This feature persists to larger mass to energy ratios (data not shown) in qualitative agreement with the opacity expansion in Fig. 2.

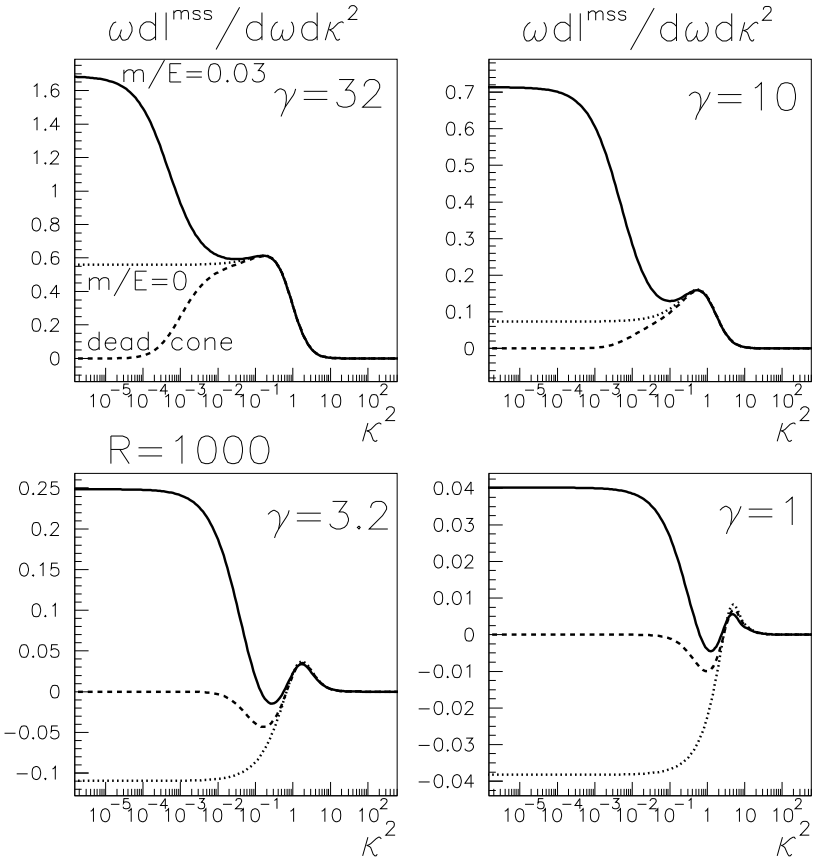

Fig. 6. The medium-induced gluon energy distribution as a function of the transverse momentum $\kappa^2 = \frac{\mathbf{k}_\perp^2}{\hat{q}L}$ and for different values of $\gamma = \omega_c/\omega$, calculated in the multiple soft scattering approximation. Different curves correspond to the full medium-induced gluon distribution for a mass to energy ratio 0.03 of the heavy quark (solid line), the massless limit of this spectrum (dotted line), and its dead cone approximation (4.15) (dashed line).

The transverse momentum integrated gluon energy distribution calculated from (4.4) is shown in Fig. 7. This integral is dominated by the phase space region $\kappa^2 > M^2$, and thus does not depend strongly on the finite medium-induced radiation inside the dead cone region. Compared to the massless case, the large-ω tail of the gluon energy distribution is depleted with increasing m/E-ratio. The approximation of this effect by the dead cone approximation (4.15) tends to underestimate this depletion. These findings are in qualitative agreement with the results reported for the opacity expansion in Fig. 3 and with the qualitative expectations based on (4.14).

We have also tested numerically the approximation of Dokshitzer and Kharzeev [25]. These authors replaced the transverse momentum dependent dead cone factor in (4.15) by an average expression, evaluated at the characteristic angle $\theta_c^2 \simeq \sqrt{2}\frac{\gamma^{3/2}}{R}$ under which medium-induced gluon radiation

occurs on average,

$$F_{\mathrm{DK}} = \left(\frac{1}{1 + \frac{1}{\sqrt{2}} \frac{m^2}{E^2} \frac{R}{\gamma^{3/2}}} \right)^2 . \tag{4.16}$$

This approximation allows to mimic the qualitative trend but is found to overestimate the depletion of the large-ω tail significantly, see Fig. 7.

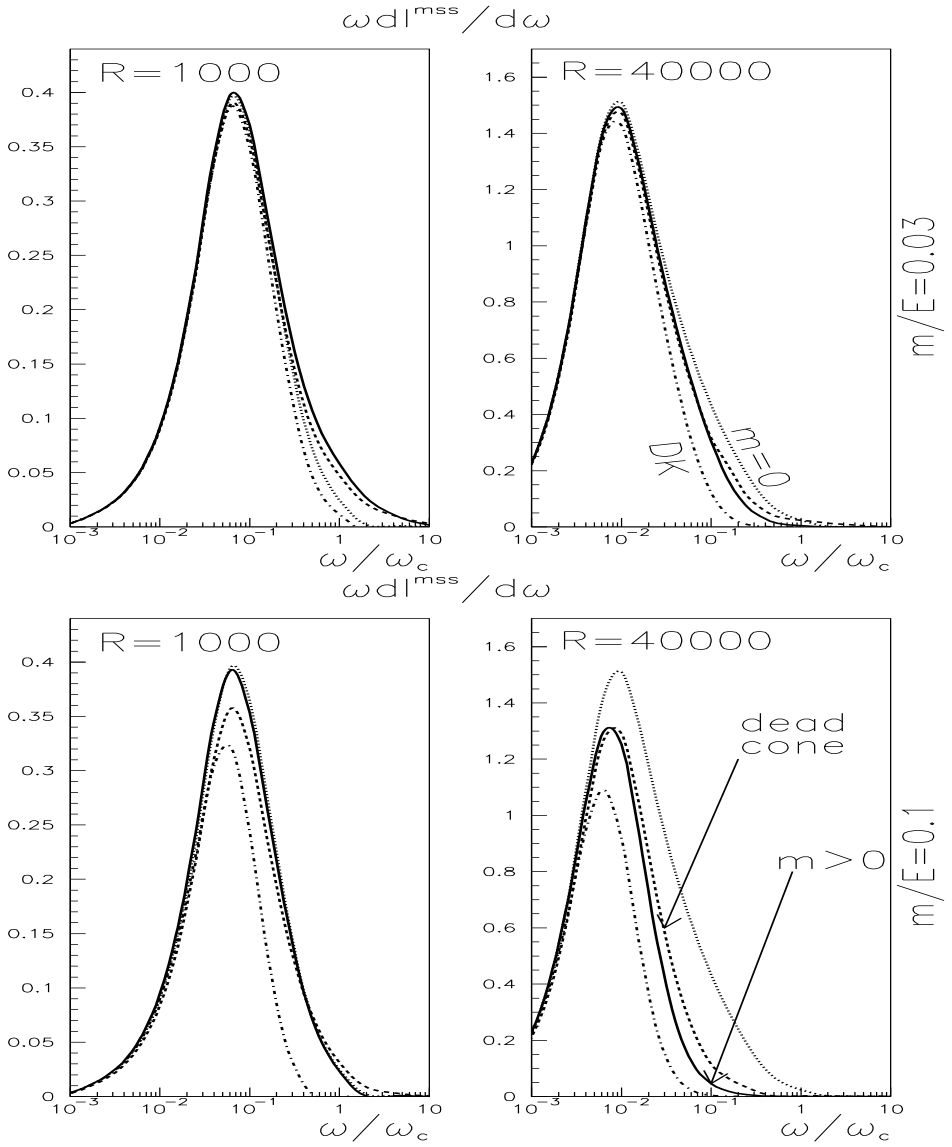

Fig. 7. Same as Fig. 3, here calculated in the multiple soft scattering approximation.

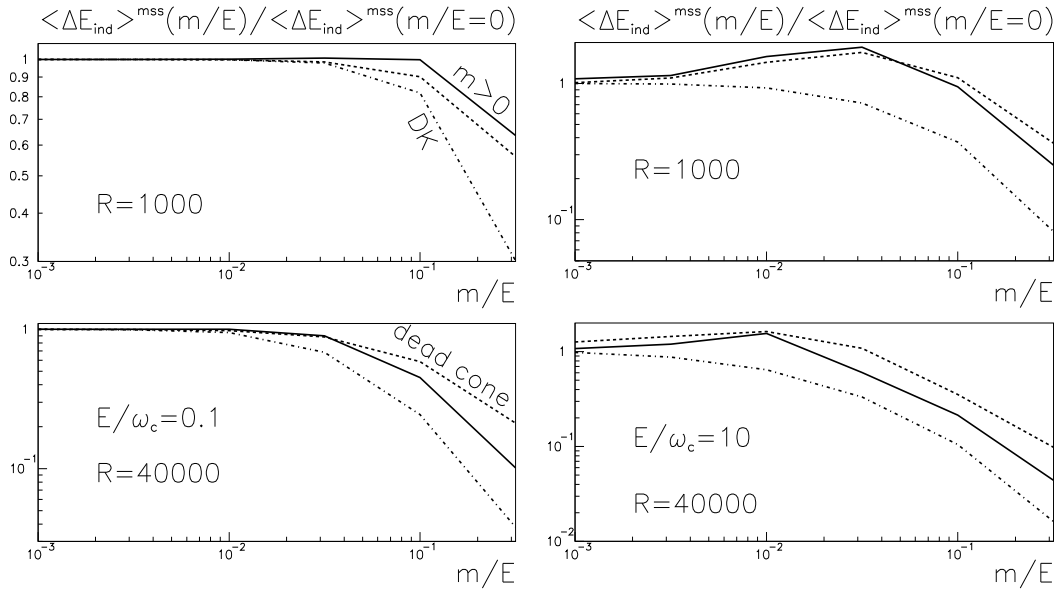

Fig. 8. Same as Fig. 4, here calculated in the multiple soft scattering approximation.

From the gluon energy distribution, we have calculated the average parton energy loss according to (3.16). As seen in Fig. 8, a finite quark mass reduces parton energy loss significantly for sufficiently large mass to energy ratios, $m/E > 0.1$ say. For smaller mass to energy ratios, there is some parameter range where our numerical results indicate the opposite effect. However, similar to the case of the opacity expansion, this may be an artifact of the phase space constraint in the definition of the average energy loss (3.16) [see the discussion of Figs. 4 and Fig. 5 above]. To explore this theoretical uncertainty, we have paralleled the logic of Section 3. We have calculated in Fig. 9 the gluon energy distribution (4.4) for the set of parameters which reproduce the nuclear modification factor for central Au+Au collisions at RHIC [23]. Integrating this gluon energy distribution for $\omega < E$, we find again that the average parton energy loss for massless quarks can be larger than that for massive ones, simply because the kinematic boundary $\omega < E$ cuts off the more pronounced large ω-tail of the gluon energy distribution for $m = 0$. For the reasons given in Section 3 C, we conclude that this motivates to go beyond the high-energy approximation and to include finite energy constraints in the calculation of $\omega \frac{dI}{d\omega}$ rather than to impose them *a posteriori* in the integral over $\omega \frac{dI}{d\omega}$.

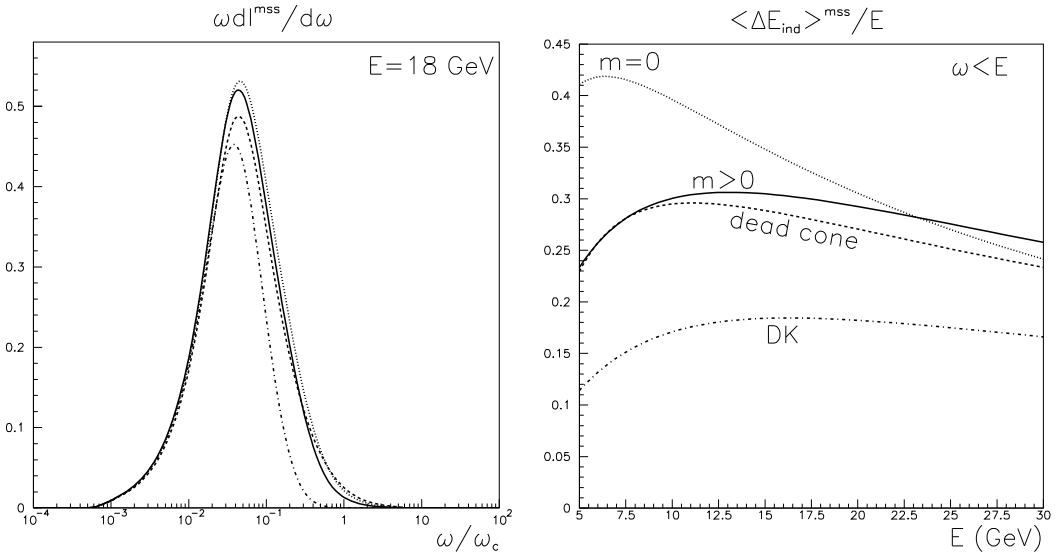

Fig. 9. Same as Fig. 5, here calculated in the multiple soft scattering approximation for parameter values $R = 2000$, $\omega_c = 67.5$ GeV and $m = 1.5$ GeV. This figure allows to illustrate the uncertainties in calculations of the average parton energy loss for finite energy quarks, see text.

5. Conclusion

Early studies demonstrated that the transverse momentum spectra of charmed and beauty hadrons in nucleus-nucleus collisions depend strongly on the assumed parton energy loss [41–43]. More recently, the quark mass dependence of this effect was argued to give access to the detailed mechanism of medium-modified parton fragmentation [25, 30–33]. To better assess this mechanism, we have presented here the first study of the transverse momentum and energy dependence of the medium-induced gluon radiation off massive quarks.

Our calculation is based on the path integral formalism (2.1) which resums medium-modifications to leading order in $1/E$ and to all orders in opacity. We have employed two approximation schemes which model the medium-dependence of the hard parton fragmentation as a series of many soft gluon exchanges or as a single semi-hard momentum transfer. Despite these different physical pictures, both approaches lead to comparable results, in agreement with an earlier study of the massless case [23].

We find that medium-induced gluon radiation generically fills the dead cone $\theta < m/E$ [see Figs. 1, 2 and 6]. However, in comparison to the transverse momentum integrated gluon energy distribution radiated off massless quarks, the radiation is depleted at large gluon energies [see Figs. 3 and 7]. The

average parton energy loss results from an interplay of both effects and tends to be smaller for massive quarks than for massless ones [see Figs. 4 and 8]. However, for sufficiently small parton energies E, the kinematic boundary $\omega < E$ can lead to the peculiar case that the average parton energy loss is larger for massive quarks than for massless ones [see Figs. 5 and 9]. We have argued that this behavior may be unphysical and limits the application of the formalism of Refs. [8–12] to sufficiently large quark energies, see discussion at the end of Section 3 C.

As of today, the only experimental information about open charm production in Au+Au collisions at RHIC is the prompt electron spectrum measured by PHENIX at $\sqrt{s_{\rm NN}} = 130$ GeV [44]. It was argued that these data do not indicate a significant parton energy loss for charm quarks. But it is equally true that they do not constrain parton energy loss significantly: First, the experimental errors on the prompt electron spectrum are still large. Second, for the measured transverse momentum range $p_\perp^{\rm electron} < 3$ GeV, the correlation between the transverse momentum of the electron and of the charmed hadron is very weak. Both complicate any conclusion about the medium-induced degradation of $p_\perp^{\rm charm}$. In addition, the moderate values of $p_\perp^{\rm charm}$ accessed by PHENIX correspond to charm quarks which move rather slowly and thus may turn into hadrons prior to leaving the collision region. In this case, the energy degradation of charmed hadrons would get contributions from their hadronic cross sections and the formalism employed here has to be revisited.

The experimental information from RHIC is expected to improve soon. First, the higher statistics of future runs will allow to measure the prompt electron spectrum in a wider $p_\perp$ range. Second, the topological reconstruction of the hadronic decay of charmed hadrons ($D^0 \to K^- \pi^+$) should provide a more direct measurement out to significant transverse momentum. On a longer time scale, open charm measurements at LHC will further extend this $p_\perp$ range to $p_\perp^{D^0} \sim 15$ GeV [45]. Also, the energy loss of beauty quarks is expected to become accessible at LHC via high-mass dimuon and secondary J/Ψ production [46]. Despite the significant uncertainties of our calculation discussed above, there is one conclusion which we can draw: parton energy loss is reduced by mass effects, but for realistic parameter values it remains sizable. Thus, our study favors a medium-induced enhancement of the D^0/π^0 ratio at sufficiently large transverse energy but we still expect the nuclear modification factor for D^0 to lie below unity.

Acknowledgment: We thank R. Baier, A. Dainese, K. Eskola, H. Honkanen, A. Morsch, G. Rodrigo and J. Schukraft for helpful discussions.

A. Gluon energy distribution to first order in opacity

In this appendix, we give details for the calculation of the zeroth and first order in opacity of the gluon energy distribution (2.1). We start by expanding the path integral in Eq. (2.1) in powers of $n(\xi)\,\sigma(\mathbf{r})$,

$$\begin{aligned}
&\mathcal{K}(\mathbf{r},y_l;\bar{\mathbf{r}},\bar{y}_l) = \mathcal{K}_0(\mathbf{r},y_l;\bar{\mathbf{r}},\bar{y}_l) \\
&-\int_z^{z'} d\xi\, n(\xi) \int d\boldsymbol{\rho}\, \mathcal{K}_0(\mathbf{r},y_l;\boldsymbol{\rho},\xi)\,\frac{1}{2}\,\sigma(\boldsymbol{\rho})\,\mathcal{K}_0(\boldsymbol{\rho},\xi;\bar{\mathbf{r}},\bar{y}_l) \\
&+\int_z^{z'} d\xi_1\, n(\xi_1) \int_{\xi_1}^{z'} d\xi_2\, n(\xi_2) \int d\boldsymbol{\rho}_1\, d\boldsymbol{\rho}_2\, \mathcal{K}_0(\mathbf{r},y_l;\boldsymbol{\rho}_1,\xi_1) \\
&\times\frac{1}{2}\,\sigma(\boldsymbol{\rho}_1)\,\mathcal{K}(\boldsymbol{\rho}_1,\xi_1;\boldsymbol{\rho}_2,\xi_2)\,\frac{1}{2}\,\sigma(\boldsymbol{\rho}_2)\,\mathcal{K}_0(\boldsymbol{\rho}_2,\xi_2;\bar{\mathbf{r}},\bar{y}_l)\,. \qquad \text{(A.1)}
\end{aligned}$$

Here, the free path integral $\mathcal{K}_0$ is of Gaussian form

$$\mathcal{K}_0(\mathbf{r},y_l;\bar{\mathbf{r}},\bar{y}_l) = \frac{\omega}{2\pi\, i\,(\bar{y}_l - y_l)} \exp\left\{\frac{i\omega\,(\bar{\mathbf{r}}-\mathbf{r})^2}{2\,(\bar{y}_l - y_l)}\right\}. \qquad \text{(A.2)}$$

We expand the integrand of (2.1) to first order in $n(\xi)\,\sigma(r)$. The longitudinal integrals in (2.1) are regularized in intermediate steps of the calculation, as explained in Ref. [10,35]. We note that the N-th order of (2.1) involves $2N+1$ terms only. This makes it straightforward to obtain explicit expressions to high orders in opacity.

Inserting (A.1) into (2.1), one finds to zeroth order opacity term (3.1). To first order in opacity, one finds

$$\begin{aligned}
\omega\frac{dI(N=1)}{d\omega\, d\mathbf{k}_\perp} = \frac{\alpha_s\, C_F}{\pi^2} 4\, n_0\, \omega \int \frac{d\mathbf{q}}{(2\pi)^2} |a(\mathbf{q})|^2\, \frac{LQ_1 - \sin(LQ_1)}{\left[(\mathbf{k}_\perp+\mathbf{q})^2 + x^2m^2\right]^2} \\
\times\left[\frac{(\mathbf{k}_\perp+\mathbf{q})^2}{(\mathbf{k}_\perp+\mathbf{q})^2+x^2m^2} - \frac{\mathbf{k}_\perp\cdot(\mathbf{k}_\perp+\mathbf{q})}{\mathbf{k}_\perp^2+x^2m^2}\right], \qquad \text{(A.3)}
\end{aligned}$$

where the transverse energy of the scattered gluon is $Q_1 = \frac{(\mathbf{k}_\perp+\mathbf{q})^2+x^2m^2}{2\omega}$.

Incoherent limit

In the totally incoherent limit, the first order opacity term (A.3) has a probabilistic parton cascade interpretation:

$$\lim_{L\to\infty} \omega\frac{dI(N=1)}{d\omega\, d\mathbf{k}_\perp}\bigg|_{n_0 L = const} = \frac{\alpha_s\, C_F}{\pi^2}(n_0\, L) \int \frac{d\mathbf{q}}{(2\pi)^2}|a(\mathbf{q})|^2$$

$$\times \left[-H(\mathbf{k}_\perp) + H(\mathbf{k}_\perp + \mathbf{q}) + R(\mathbf{k}_\perp, \mathbf{q})\right] . \quad \text{(A.4)}$$

Here, $H(\mathbf{k}_\perp)$ is multiplied by the probability that the hard parton interacts with the medium; the minus sign ensures probability conservation by reducing the corresponding weight of the $N = 0$ vacuum contribution (3.1). For a scattering center far away from the point of quark production, interaction with the medium gives rise to two processes: i) The vacuum radiation term $H(\mathbf{k}_\perp)$ is shifted to $H(\mathbf{k}_\perp + \mathbf{q})$ due to medium-induced elastic scattering by a transverse momentum $\mathbf{q}$. ii) Gluons are produced due to bremsstrahlung off the far distant scattering center. This leads to the Gunion-Bertsch radiation term for massive quarks,

$$R(\mathbf{k}_\perp, \mathbf{q}) = \frac{(\mathbf{k}_\perp + \mathbf{q})^2}{[(\mathbf{k}_\perp + \mathbf{q})^2 + x^2 m^2]^2} - \frac{2\,\mathbf{k}_\perp \cdot (\mathbf{k}_\perp + \mathbf{q})}{[(\mathbf{k}_\perp + \mathbf{q})^2 + x^2 m^2]\,[\mathbf{k}_\perp^2 + x^2 m^2]} + \frac{\mathbf{k}_\perp^2}{[\mathbf{k}_\perp^2 + x^2 m^2]^2} . \quad \text{(A.5)}$$

For realistic, finite in-medium pathlength, both effects combine in the specific interference pattern (A.3).

$\underline{N = 1 \text{ opacity term for Yukawa-type scattering potential:}}$
We have studied (A.3) for arbitrary in-medium pathlength for a Yukawa-type elastic scattering center with Debye screening mass μ:

$$|a(\mathbf{q})|^2 = (2\pi)^2 \frac{\mu^2}{\pi(\mathbf{q}^2 + \mu^2)^2} . \quad \text{(A.6)}$$

Shifting in (A.3) the relative momentum integration $\mathbf{q} \to \mathbf{q} + \mathbf{k}$ and doing the angular integrations, one finds

$$\omega \frac{dI(N=1)}{d\omega\, dk^2} = \frac{\alpha_s C_F}{\pi} \frac{n_0\, \mu^2}{\omega} \int_0^\infty dq^2 \frac{LQ_1' - \sin(LQ_1')}{Q_1'^2} \frac{q^2}{q^2 + x^2 m^2} \times \frac{\mu^2 (k^2 + x^2 m^2) + (k^2 - x^2 m^2)(k^2 - q^2)}{(k^2 + x^2 m^2)\left[(m^2 + k^2 + q^2)^2 - 4k^2 q^2\right]^{3/2}} , \quad \text{(A.7)}$$

where $Q_1' = \frac{\mathbf{q}^2 + x^2 m^2}{2\omega}$. From this expression, we find Eq. (3.14) by rescaling the variables ω, k^2 and m^2 to the dimensionless variables $\bar{\gamma}$, $\bar{\kappa}^2$ and $\bar{M}^2$ defined in eqs. (3.4), (3.7) and (3.11) respectively.

B. Gluon energy distribution in the dipole approximation

Here, we give the full expression for the medium-induced part of the double differential gluon distribution (4.4). The calculation is done in complete analogy to the calculation of the massless case [20], but keeping the mass-dependence of (2.1). In the rescaled dimensionless variables introduced in Section 4, one finds

$$\omega\frac{dI_4}{d\omega\,d\kappa^2} = \frac{\alpha_s\,C_F}{\pi}\gamma^2\,2\,\mathrm{Re}\int_0^1 dt\int_t^1 d\bar{t}\,e^{i\,M^2\,\gamma\,(t-\bar{t})}\exp\left[-\frac{\kappa^2}{4(D_4-iA_4B_4)}\right] \times\left[\frac{iA_4^3\,B_4\,\kappa^2}{(D_4-iA_4B_4)^3}-\frac{4A_4^2D_4}{(D_4-iA_4B_4)^2}\right], \tag{B.1}$$

where

$$\Omega = \frac{1-i}{\sqrt{2}}\sqrt{\gamma} \tag{B.2}$$

and

$$A_4 = \frac{\Omega}{4\gamma\,\sin\left[\Omega(\bar{t}-t)\right]}, \quad B_4 = \cos\left[\Omega(\bar{t}-t)\right], \quad D_4 = \frac{1}{4}\,(1-\bar{t})\,. \tag{B.3}$$

The term I_5 in Eq. (4.2) takes the form

$$\omega\frac{dI_5}{d\omega\,d\kappa^2} = \frac{\alpha_s\,C_F}{\pi}\gamma\,2\,\mathrm{Re}\int_0^1 dt\,e^{-i\,M^2\,\gamma\,t}\left(\frac{-i\kappa^2}{\kappa^2+M^2}\right) \times\frac{1}{B_5^2}\exp\left[-\frac{i\kappa^2}{4\,A_5\,B_5}\right], \tag{B.4}$$

where

$$A_5 = \frac{\Omega}{4\gamma\,\sin\left[\Omega\,t\right]}, \quad B_5 = \cos\left[\Omega\,t\right]\,. \tag{B.5}$$

---

1. Y. L. Dokshitzer, V. A. Khoze and S. I. Troian, J. Phys. G **17** (1991) 1481.
2. K. Ackerstaff *et al.* [OPAL Collaboration], Eur. Phys. J. C **7** (1999) 369 [arXiv:hep-ex/9807004].

3. D. Buskulic *et al.* [ALEPH Collaboration], Z. Phys. C **62** (1994) 1.
4. G. Abbiendi *et al.* [OPAL Collaboration], arXiv:hep-ex/0210031.
5. B. A. Schumm, Y. L. Dokshitzer, V. A. Khoze and D. S. Koetke, Phys. Rev. Lett. **69** (1992) 3025.
6. S. Gieseke, P. Stephens and B. Webber, arXiv:hep-ph/0310083.
7. M. Gyulassy and X. N. Wang, Nucl. Phys. B **420** (1994) 583 [arXiv:nucl-th/9306003].
8. R. Baier, Y. L. Dokshitzer, A. H. Mueller, S. Peigne and D. Schiff, Nucl. Phys. B **484** (1997) 265 [arXiv:hep-ph/9608322].
9. B. G. Zakharov, JETP Lett. **65** (1997) 615 [arXiv:hep-ph/9704255].
10. U. A. Wiedemann, Nucl. Phys. B **588** (2000) 303 [arXiv:hep-ph/0005129].
11. M. Gyulassy, P. Levai and I. Vitev, Nucl. Phys. B **594** (2001) 371 [arXiv:nucl-th/0006010].
12. X. N. Wang and X. f. Guo, Nucl. Phys. A **696** (2001) 788 [arXiv:hep-ph/0102230].
13. K. Adcox *et al.* [PHENIX Collaboration], Phys. Rev. Lett. **88** (2002) 022301 [arXiv:nucl-ex/0109003].
14. S. S. Adler [PHENIX Collaboration], arXiv:nucl-ex/0308006.
15. C. Adler *et al.* [STAR Collaboration], Phys. Rev. Lett. **89** (2002) 202301 [arXiv:nucl-ex/0206011].
16. J. Adams *et al.* [STAR Collaboration], Phys. Rev. Lett. **91** (2003) 172302 [arXiv:nucl-ex/0305015].
17. B. B. Back *et al.* [PHOBOS Collaboration], arXiv:nucl-ex/0302015.
18. I. Arsene *et al.* [BRAHMS Collaboration], Phys. Rev. Lett. **91** (2003) 072305 [arXiv:nucl-ex/0307003].
19. X. N. Wang, arXiv:nucl-th/0307036.
20. U. A. Wiedemann, Nucl. Phys. A **690** (2001) 731 [arXiv:hep-ph/0008241].
21. R. Baier, Y. L. Dokshitzer, A. H. Mueller and D. Schiff, Phys. Rev. C **60** (1999) 064902 [arXiv:hep-ph/9907267].
22. R. Baier, Y. L. Dokshitzer, A. H. Mueller and D. Schiff, Phys. Rev. C **64** (2001) 057902 [arXiv:hep-ph/0105062].
23. C. A. Salgado and U. A. Wiedemann, Phys. Rev. D **68** (2003) 014008 [arXiv:hep-ph/0302184].
24. C. A. Salgado and U. A. Wiedemann, arXiv:hep-ph/0310079.
25. Yu. L. Dokshitzer and D. E. Kharzeev, Phys. Lett. B **519** (2001) 199 [arXiv:hep-ph/0106202].
26. K. J. Eskola, V. J. Kolhinen and R. Vogt, arXiv:hep-ph/0310111.
27. F. Gelis and R. Venugopalan, arXiv:hep-ph/0310090.
28. D. Kharzeev and K. Tuchin, arXiv:hep-ph/0310358.
29. A. Accardi *et al.*, arXiv:hep-ph/0308248.
30. M. Djordjevic and M. Gyulassy, Phys. Lett. B **560** (2003) 37 [arXiv:nucl-th/0302069].
31. M. Djordjevic and M. Gyulassy, Phys. Rev. C **68** (2003) 034914 [arXiv:nucl-th/0305062].
32. M. Djordjevic and M. Gyulassy, arXiv:nucl-th/0310076.
33. B. W. Zhang, E. Wang and X. N. Wang, arXiv:nucl-th/0309040.
34. B. G. Zakharov, JETP Lett. **63** (1996) 952 [arXiv:hep-ph/9607440].

35. U. A. Wiedemann and M. Gyulassy, Nucl. Phys. B **560** (1999) 345 [arXiv:hep-ph/9906257].
36. C. A. Salgado and U. A. Wiedemann, Phys. Rev. Lett. **89** (2002) 092303 [arXiv:hep-ph/0204221].
37. M. Gyulassy, P. Levai and I. Vitev, Phys. Rev. Lett. **85** (2000) 5535 [arXiv:nucl-th/0005032].
38. P. Levai, G. Papp, G. Fai, M. Gyulassy, G. G. Barnafoldi, I. Vitev and Y. Zhang, Nucl. Phys. A **698** (2002) 631 [arXiv:nucl-th/0104035].
39. B. G. Zakharov, Phys. Atom. Nucl. **61** (1998) 838 [Yad. Fiz. **61** (1998) 924] [arXiv:hep-ph/9807540].
40. R. Baier, Nucl. Phys. A **715** (2003) 209 [arXiv:hep-ph/0209038].
41. E. V. Shuryak, Phys. Rev. C **55** (1997) 961 [arXiv:nucl-th/9605011].
42. Z. w. Lin, R. Vogt and X. N. Wang, Phys. Rev. C **57** (1998) 899 [arXiv:nucl-th/9705006].
43. M. G. Mustafa, D. Pal, D. K. Srivastava and M. Thoma, Phys. Lett. B **428** (1998) 234 [arXiv:nucl-th/9711059].
44. K. Adcox *et al.* [PHENIX Collaboration], Phys. Rev. Lett. **88** (2002) 192303 [arXiv:nucl-ex/0202002].
45. A. Dainese, arXiv:nucl-ex/0312005.
46. I. P. Lokhtin and A. M. Snigirev, J. Phys. G **27** (2001) 2365.